Near-Field Nonlinear Microwave Microscope for Fundamental Superconducting Studies

Chung-Yang Wang, Steven M. Anlage

Quantum Materials Center, Department of Physics, University of Maryland, College Park, USA

chyawang@terpmail.umd.edu, anlage@umd.edu

Abstract — **This article presents the implementation of a near-field magnetic microwave microscope integrated into a cryostat with a base temperature of 3.6 K. The probe of the microwave microscope is a magnetic writer capable of generating a strong microwave magnetic field within a sub-micron region. A microwave signal in the GHz range is directed to the magnetic writer. The magnetic writer then generates a local RF field to stimulate the superconducting sample. The sample creates screening currents and the local response is collected by the same magnetic writer. Nonlinear components of the sample response, particularly the third harmonic response, are extracted using a spectrum analyzer. We employ this microwave microscope to investigate a Nb film, a type-II superconductor with a transition temperature around 9.3 K. By analyzing the third harmonic response of the Nb film, we explore the sample's surface defects, especially those that nucleate RF magnetic vortices.**

Keywords — **harmonics, scanning microwave microscopy, superconductivity.**

I. INTRODUCTION

Microwave microscopy is a near-field imaging technique that has been used to study inhomogeneous electromagnetic properties with nanoscale resolution across the GHz regime [1]. Operating in the near-field regime, this technique achieves nanoscale resolution beyond the diffraction limit by bringing a sharp probe into close proximity to the sample. Microwave microscopy typically functions in reflectometry mode, where microwaves are transmitted to the sample through the sharp (enhanced electric field) probe, and the reflected signal is measured. It is widely used for imaging local dielectric permittivity and electrical conductivity of high-impedance samples [2–5].

When a material undergoes a slight perturbation from an electromagnetic field, its response is primarily linear. This category includes the measurement of local dielectric permittivity and electrical conductivity. In contrast, when the electromagnetic field is strong enough to significantly influence the material, the response becomes nonlinear. Such nonlinear response provides insights that are not captured by linear response measurements. Specifically, in the case of a type-II superconductor driven by a strong RF magnetic field, the material nucleates RF vortices, leading to a strong third harmonic response [6–11], which makes it a valuable tool for studying phenomena related to RF vortex nucleation.

In this work, we report the implementation of a cryogenic near-field magnetic microwave microscope. The microscope is designed to explore the nonlinear response of superconductors in the GHz regime. To demonstrate the measurement capabilities of this setup, we present the third harmonic response measurement of a Nb film, a type-II superconductor with a transition temperature of around 9.3 K. By analyzing the temperature dependence of the third harmonic response of the Nb film, the sample's surface defects are revealed, especially those associated with the nucleation of RF magnetic vortices. The understanding of microwave properties associated with surface defects is crucial for optimizing the performance of superconductors in various applications, including superconducting radio-frequency (SRF) cavities [12].

II. EXPERIMENTAL SETUP

The setup of our near-field magnetic microwave microscope consists of a magnetic writer probe integrated into a dry cryostat. A schematic of the setup is shown in Fig. 1.

The cryostat (represented by the green dashed box in Fig. 1(a)) has three plates: a room temperature top plate, a 70 K plate, and a 4 K cold plate. Each plate is equipped with a corresponding vacuum can. The microscope head is positioned below, and thermally anchored to, the cold plate. The superconducting sample and the thermometer (close to the sample) are both directly mounted on the cold plate to ensure good thermalization. The base temperature for a sample in the cryostat is around 3.6 K.

The heart of our microwave microscope is the magnetic writer probe (provided by Seagate Technology) that is designed for magnetic reading and writing in conventional hard disk drives [13]. Fig. 1(b) displays a photograph of the magnetic writer probe. The probe is engineered to operate with GHz bandwidth. The probe consists of a slider, transmission lines, and an aluminum assembly that holds the slider and the transmission lines together. The slider, enclosed within the yellow dashed box in Fig. 1(b), houses the magnetic writer head, which is the primary component of the probe. The magnetic writer head is capable of generating a localized RF magnetic field, which makes it particularly suitable for our microwave microscope. Fig. 1(c) shows a scanning electron microscope (SEM) image of the magnetic writer head. The magnetic shielding near the magnetic writer head is enclosed in the yellow circle. The yellow box provides a magnified view, specifically focusing on the magnetic writer head. The size of the magnetic writer head is in the sub-micron scale, which sets the spatial resolution of our microscope.

In the experimental setup, a Seagate magnetic writer head is attached to a cryogenic XYZ positioner (with sub-micron spatial resolution) and employed in a scanning probe microscope fashion. During the third harmonic measurement, the probe makes contact with the sample. However, the surfaces of the probe and sample are not perfectly flat, resulting in a finite probe-sample separation h, estimated to be less than 1 micron. The peak microwave magnetic field experienced by the sample is estimated to be in the range of tens of mT for a 0 dBm input microwave power.

A schematic of the RF circuit setup is presented in Fig. 1(a). The process begins with the production of a microwave signal at frequency f by a microwave source (Keysight N5173B). This signal is then directed to the magnetic writer probe inside the cryostat through a series connection of coaxial cables. Notably, these include room-temperature coaxial cables outside the cryostat and cryogenic coaxial cables inside the cryostat. Thermal anchoring of the coaxial cables within the cryostat is ensured as they pass through the 70 K plate and the 4 K cold plate. The coaxial cable terminates with an SMA coaxial connector, which is directly soldered to the pads on the end of the magnetic writer probe transmission lines. The probe then produces a local RF magnetic field $B_{RF}sin(\omega t)$ that acts on the sample surface. In response, the superconducting sample generates a screening current on the surface in an effort to maintain the Meissner state. The magnetic field associated with this screening current is then coupled back to the same probe, creating a return propagating signal on the transmission line structure. This response signal shares the same cryogenic coaxial cables with the input signal and is branched out by a directional coupler at room temperature. The amplitude of the third harmonic component $P_{3f}sin^2(3\omega t)$ is projected out with a spectrum analyzer (Agilent E4407B) at room temperature. A 10 MHz reference signal is generated by the microwave source and sent to the spectrum analyzer in order to synchronize the two instruments.

To improve the signal-to-noise ratio, microwave filters are deployed in the following manner. First, low-pass filters are installed between the microwave source and the probe. These filters effectively block unwanted harmonic signals generated by the microwave source. Given that the response signal comprises both linear and nonlinear components, the next step involves the installation of high-pass filters between the probe and the spectrum analyzer. This placement prevents the fundamental input frequency signal (linear response [14]) from reaching the spectrum analyzer, thereby mitigating the generation of unwanted nonlinear signals. The frequency windows of the low-pass filters and the high-pass filters are 0 - 2.2 GHz and 2.9 - 8.7 GHz, respectively. The input frequency f is selected to fall within the range of 1.1 GHz to 2.2 GHz based on these frequency windows. This strategic choice ensures optimal filtering conditions and contributes to the overall improvement of the signal-to-noise ratio. This frequency range also includes the operating frequency of superconducting radio-frequency Nb accelerator cavities [12].

The magnetic writer head, serving as the probe in our microwave microscope, is composed of magnetic materials that exhibit nonlinearity, constituting the primary background signal (probe background) in the measurements of nonlinear response. The probe background is temperature-independent, as confirmed both by P_{3f} measurements when the probe is not in contact with the superconducting sample and by P_{3f} measurements of a copper sample. The P_{3f} measured by the spectrum analyzer is the combination of the probe background and the response of the superconducting sample. Because the third harmonic response of the superconducting sample typically exhibits a nontrivial temperature dependence, it can be distinguished from the temperature-independent probe background by measuring P_{3f} as a function of temperature.

The P_{3f} measurements of superconductor nonlinear response exhibit an impressive dynamic range, often surpassing 20 dB [6–8]. The excellent instrumental nonlinear background of our measurements (approximately -155 dBm) enables highly sensitive measurements of superconductor nonlinearity and its variation with temperature, driving RF power, location, and probe-sample separation.

III. Experimental Results

In this work, we investigate a Nb film with a thickness of approximately 1.2 μm deposited on a Cu substrate. The sample is prepared at CERN [15].

Fig. 2 displays the representative data illustrating the third harmonic response power P_{3f} as a function of temperature at a fixed location on the Nb/Cu sample. The measurement
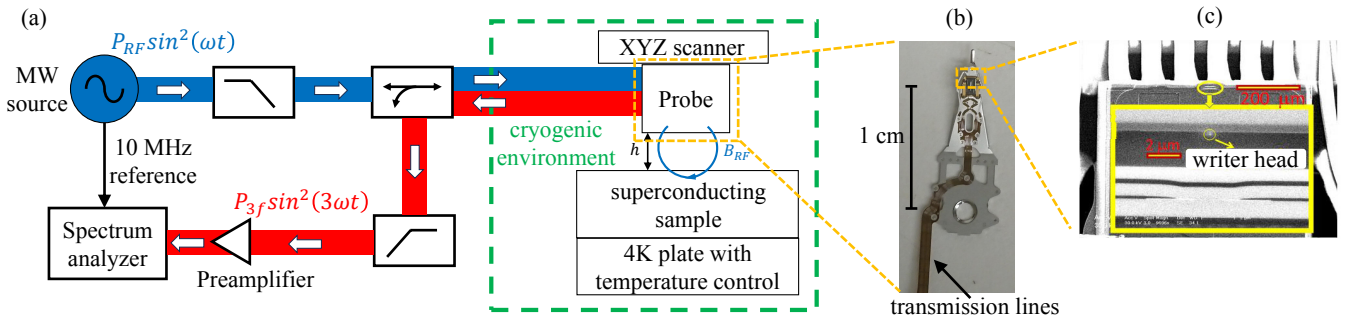

Fig. 1. Near-field magnetic microwave microscope integrated into a dry cryostat. (a) Schematic of the microwave microscope, including the room temperature part and the cryogenic part. (b) Photograph of the magnetic writer probe. (c) SEM image of the magnetic writer head.
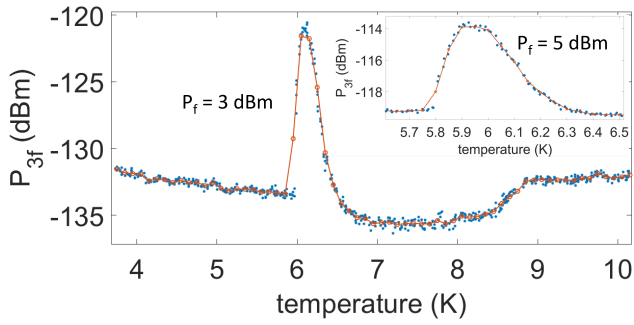
Fig. 2. Representative data for the variation of P_{3f} with temperature at a fixed location on the Nb/Cu sample, with an input frequency of 2.16 GHz and an input power of 3 dBm. The inset shows P_{3f} with an input power of 5 dBm and focuses on the peak around 6 K.
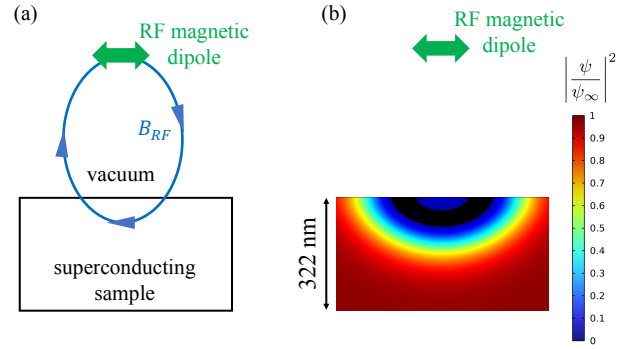

Fig. 3. RF dipole model. (a) Schematic of the RF magnetic field generated by an RF magnetic point dipole. (b) Snapshot of the square of the normalized order parameter of Nb obtained from a time-dependent Ginzburg-Landau simulation. In the image, the black region corresponds to where $|\psi/\psi_\infty|^2 < 0.03$. The RF magnetic dipole is 400 nm above the Nb sample. The RF magnetic field used in the simulation has a frequency of 1.7 GHz and a peak magnetic field strength of 61.6 mT. The temperature is 8.23 K.

protocol involves initially warming the sample above its critical temperature (T_c) to 10 K. Subsequently, the microwave source is activated with a constant input frequency ($f = \omega/2\pi$=2.16 GHz) and input power (P_{RF}=+3 dBm). P_{3f} is then measured as the sample is gradually cooled to 3.6 K. This process ensures that the surface of the sample experiences a fixed RF field $B_{RF}sin(\omega t)$ in a sub-micron scale area throughout the cooldown from 10 K to 3.6 K.

The measured $P_{3f}(T)$ in Fig. 2 exhibits three distinct segments: the region above 8.9 K, the region below 6.4 K, and the region in between. The nonlinearity of the magnetic writer head (probe background) contributes to P_{3f} above 8.9 K, and this background signal is indeed temperature-independent. Superconductors exhibit intrinsic nonlinear response around T_c [6–9, 11]. Indeed, a transition of P_{3f} occurs around 8.9 K, which corresponds to the intrinsic nonlinear response of the Nb film. The measured P_{3f} is the complex vector superposition of the probe background and the sample response. If these components are out of phase [7], the total signal would be weaker than the probe background. This explains why the signal at 8 K is observed to be weaker than that at 9 K. The onset of the strongest P_{3f} signal is observed around 6.4 K, presenting a dramatic contrast to the signal around 8.9 K. This signal suggests the emergence of a mechanism at and below 6.4 K that contributes to strong nonlinearity. The mechanism leading to strong P_{3f} below 6.4 K is clearly distinct from the signal due to intrinsic Nb response, which implies that the mechanism is extrinsic and is likely due to surface defects that nucleate RF vortices. Note that P_{3f} below 6.4 K is much stronger than the intrinsic Nb signal around 8.9 K, indicating that our near-field nonlinear microwave microscope is sensitive to surface defects.

$P_{3f}(T)$ is measured for another input power (P_{RF}=+5 dBm) using the same measurement protocol, and the result is presented in the inset of Fig. 2. The peak of $P_{3f}(T)$ occurs at approximately 6.10 K for P_{RF}=+3 dBm and around 5.95 K for P_{RF}=+5 dBm. Notably, the peak of $P_{3f}(T)$ shifts to a lower temperature with increasing input power, a behavior consistent with the nonlinear response created by RF vortex nucleation [11].

IV. DISCUSSION

The magnetic writer probe is engineered for use in conventional hard disk drives. In this application, it flips domains in a magnetized medium and creates permanent changes to the medium. In our microwave microscope, the probe is placed in a cryogenic environment and stimulated with GHz signals, and the material beneath the probe is a superconductor rather than a magnetized medium. In the following, we explore how the superconductor responds when stimulated by the RF magnetic field generated by the probe.

The magnetic field generated by the magnetic writer head has both a longitudinal component and a perpendicular component [13]. The specific configuration of this magnetic field depends on the detailed design of the magnetic writer, which is beyond the scope of our current study. Our focus is on utilizing a magnetic field that incorporates both the longitudinal and perpendicular components. For this purpose, the magnetic field of a point dipole oriented parallel to the superconducting surface serves as a suitable approximation for the magnetic field generated by the magnetic writer probe. Fig. 3(a) is a schematic of an RF magnetic dipole positioned above a superconducting sample. The blue curve (B_{RF}) represents the RF magnetic field generated by the RF magnetic dipole. Given that the RF magnetic field experienced by the superconducting sample includes both a longitudinal component and a perpendicular component, this RF dipole model is considered a good approximation of the magnetic field distribution underneath the magnetic writer head.

Type-II superconductors are in the vortex-free Meissner state when the applied magnetic field is weaker than the first critical field. When the applied magnetic field exceeds the first critical field, vortices nucleate in type-II superconductors. In the context of an RF magnetic field $B_{RF}sin(\omega t)$, these vortices are transient and short-lived, appearing and disappearing twice per RF cycle, and are referred to as RF vortices [9–11].

The dynamics of RF vortices can be investigated using the time-dependent Ginzburg-Landau (TDGL) model [9–11]. Here we conduct a TDGL simulation for Nb. The RF magnetic dipole is positioned 400 nm above the Nb sample. The RF field generated by the RF magnetic dipole has a frequency of 1.7 GHz, and the peak magnetic field experienced by the Nb is 61.6 mT. The simulation is performed at a temperature of 8.23 K. Fig. 3(b) is a snapshot when the RF magnetic field $B_{RF}sin(\omega t)$ reaches the maximum ($\omega t = \pi/2$). The color represents the strength of superconductivity: red means fully superconducting, blue means superconductivity being suppressed, and black means superconductivity being significantly suppressed. In this snapshot, a distinctive feature is the presence of an RF vortex semi-loop in the Nb. Note that superconductivity is significantly suppressed inside the core of a vortex, represented by the black region.

The RF vortex semi-loop shown in Fig. 3(b) is transient, appearing and disappearing twice per RF cycle. This transient behavior contrasts with the permanent domain flip of a magnetized medium in hard disk drives when stimulated by the magnetic field of the magnetic writer probe. In our microwave microscope, the superconducting sample undergoes only transient changes, characterized by the alternating suppression and recovery of the superconducting order parameter and the generation of transient RF vortex semi-loops.

Superconductors exhibit relatively weak nonlinearity in the vortex-free Meissner state and exhibit strong nonlinearity in the presence of vortices [6–9, 11, 16]. Therefore, by measuring the third harmonic response of superconductors, we explore phenomena related to the nucleation of RF vortex semi-loops. A superconductor may have surface defects (oxides, grain boundaries, dislocations, etc.) acting as extrinsic mechanisms of vortex nucleation. When the superconductor is subjected to an RF field exceeding the effective vortex penetration field around the surface defects, RF vortices can nucleate at these surface defects, resulting in a strong third harmonic response.

The strong P_{3f} observed below 6.4 K shown in Fig. 2 is clearly distinguished from the signal associated with the intrinsic Nb response. This separation implies that the strong P_{3f} likely originates from RF vortex nucleation at surface defects of the Nb/Cu sample.

V. Conclusion

In this report, we present the development of a cryogenic near-field nonlinear microwave microscope designed for measuring the third harmonic response of superconductors. This involves integrating a magnetic writer probe into a dry cryostat. Utilizing the microwave microscope, we explore a Nb/Cu film, and the analysis of its temperature-dependent third harmonic response reveals surface defects that nucleate RF vortices. These findings offer crucial insights into microwave properties for optimizing the performance of superconductors across diverse applications.

References

[1] S. M. Anlage, V. V. Talanov, and A. R. Schwartz, "Principles of near-field microwave microscopy," in *Scanning Probe Microscopy: Electrical and Electromechanical Phenomena at the Nanoscale*. Springer, 2007, pp. 215–253.

[2] D. Steinhauer, C. Vlahacos, S. Dutta, B. Feenstra, F. Wellstood, and S. M. Anlage, "Quantitative imaging of sheet resistance with a scanning near-field microwave microscope," *Applied Physics Letters*, vol. 72, no. 7, pp. 861–863, 1998.

[3] D. Steinhauer, C. Vlahacos, F. Wellstood, S. M. Anlage, C. Canedy, R. Ramesh, A. Stanishevsky, and J. Melngailis, "Quantitative imaging of dielectric permittivity and tunability with a near-field scanning microwave microscope," *Review of Scientific Instruments*, vol. 71, no. 7, pp. 2751–2758, 2000.

[4] A. Tselev, S. M. Anlage, Z. Ma, and J. Melngailis, "Broadband dielectric microwave microscopy on micron length scales," *Review of Scientific Instruments*, vol. 78, no. 4, p. 044701, 04 2007.

[5] X. Wu, Z. Hao, D. Wu, L. Zheng, Z. Jiang, V. Ganesan, Y. Wang, and K. Lai, "Quantitative measurements of nanoscale permittivity and conductivity using tuning-fork-based microwave impedance microscopy," *Review of Scientific Instruments*, vol. 89, no. 4, p. 043704, 2018.

[6] S.-C. Lee, S.-Y. Lee, and S. M. Anlage, "Microwave nonlinearities of an isolated long $YBa_2Cu_3O_{7-\delta}$ bicrystal grain boundary," *Physical Review B*, vol. 72, no. 2, p. 024527, 2005.

[7] D. I. Mircea, H. Xu, and S. M. Anlage, "Phase-sensitive harmonic measurements of microwave nonlinearities in cuprate thin films," *Physical Review B*, vol. 80, no. 14, p. 144505, 2009.

[8] T. Tai, B. G. Ghamsari, T. Bieler, and S. M. Anlage, "Nanoscale nonlinear radio frequency properties of bulk Nb: Origins of extrinsic nonlinear effects," *Physical Review B*, vol. 92, no. 13, p. 134513, 2015.

[9] B. Oripov, T. Bieler, G. Ciovati, S. Calatroni, P. Dhakal, T. Junginger, O. B. Malyshev, G. Terenziani, A.-M. Valente-Feliciano, R. Valizadeh *et al.*, "High-frequency nonlinear response of superconducting cavity-grade Nb surfaces," *Physical Review Applied*, vol. 11, no. 6, p. 064030, 2019.

[10] B. Oripov and S. M. Anlage, "Time-dependent Ginzburg-Landau treatment of rf magnetic vortices in superconductors: Vortex semiloops in a spatially nonuniform magnetic field," *Physical Review E*, vol. 101, no. 3, p. 033306, 2020.

[11] C.-Y. Wang, C. Pereira, S. Leith, G. Rosaz, and S. M. Anlage, "Microscopic examination of SRF-quality Nb films through local nonlinear microwave response," *ArXiv preprint arXiv:2305.07746*, 2023.

[12] H. Padamsee, "50 years of success for SRF accelerators—a review," *Superconductor Science and Technology*, vol. 30, no. 5, p. 053003, 2017.

[13] B. Bhushan, "Current status and outlook of magnetic data storage devices," *Microsystem Technologies*, vol. 29, pp. 1529–1546, 2023.

[14] T. Tai, B. Ghamsari, and S. M. Anlage, "Modeling the nanoscale linear response of superconducting thin films measured by a scanning probe microwave microscope," *Journal of Applied Physics*, vol. 115, no. 20, p. 203908, 2014.

[15] M. Ghaemi, A. Lopez-Cazalilla, K. Sarakinos, G. Rosaz, C. Carlos, S. Leith, S. Calatroni, M. Himmerlich, and F. Djurabekova, "Growth of Nb films on Cu for superconducting radio frequency cavities by direct current and high power impulse magnetron sputtering: A molecular dynamics and experimental study," *Surface and Coatings Technology*, vol. 476, p. 130199, 2024.

[16] G. Lamura, M. Aurino, A. Andreone, and J.-C. Villégier, "First critical field measurements of superconducting films by third harmonic analysis," *Journal of Applied Physics*, vol. 106, no. 5, p. 053903, 2009.